FISEVIER

Contents lists available at ScienceDirect

Journal of Membrane Science

journal homepage: www.elsevier.com/locate/memsci



Forward osmosis desalination of oil and gas wastewater: Impacts of membrane selection and operating conditions on process performance



Bryan D. Coday, Nohemi Almaraz, Tzahi Y. Cath*

Colorado School of Mines, 1500 Illinois St., Golden, CO 80401, USA

ARTICLE INFO

Article history:
Received 19 January 2015
Received in revised form
17 March 2015
Accepted 18 March 2015
Available online 10 April 2015

Keywords:
Forward osmosis
Produced water
Fracturing flowback
Wastewater treatment
Membrane fouling

ABSTRACT

Water treatment technologies that employ sustainable driving forces for treatment of high ionic strength, complex feed streams and have the capacity to separate a broad range of contaminants are needed for economical treatment of flowback and produced waters in the oil and gas industry. This is especially true given the surging interest in treatment of oil and gas wastewaters for reuse in hydraulic fracturing or discharge to the environment in lieu of deep well injection. Forward osmosis is a robust membrane separation technology that can provide superior rejection of a broad range of feed stream contaminants and dissolved ions, thus providing a brine stream suitable for reuse in hydraulic fracturing or excellent pretreatment for downstream desalination processes. In this work, the impacts of membrane selection (asymmetric cellulose triacetate versus polyamide thin-film composite) and system operating conditions on the performance of FO membranes for desalination of produced water for the Niobrara shale formation are investigated. Specifically, water flux, contaminant rejection, membrane fouling, and chemical cleaning were evaluated using a combination of standard methodology and operating conditions analogous to those employed when operating industrial spiral wound FO membrane modules. Membrane autopsy was conducted to determine what effect(s) membrane physiochemical properties might have on system performance and to interpret the potential molecular level interactions occurring near the membrane-feed stream interface. Results from this study indicate that FO can achieve high rejection of organic and inorganic contaminants, membrane fouling can be mitigated with chemical cleaning, and long-term FO system performance might be better controlled with optimized hydrodynamic conditions near the membrane surface (i.e., feed flow velocity, module design, membrane packing) and not by membrane selection.

© 2015 Elsevier B.V. All rights reserved.

1. Introduction

1.1. Hydraulic fracturing flowback and produced water in unconventional oil and gas

Hydraulic fracturing flowback and produced water are complex industrial waste streams resulting from the exploration and development of unconventional oil and gas (0&G) resources. During hydraulic fracturing a water-based slurry, typically in the range of 4 million gallons, is injected into the oil or gas well under extremely high pressures [1–3]. This process fractures the subsurface 0&G formation, effectively increasing the permeability of the reservoir and enhancing recovery of hydrocarbons. The hydraulic fracturing process occurs after a well has been drilled and can be repeated several times throughout the service life of the well. After

the fracturing process has been completed, a portion of the fracturing fluids are recovered from the well for up to a month, generating an industrial waste stream (commonly termed "flow-back water") consisting of water, proppants (i.e., silica, graded sand or ceramic materials), chemical additives, and a variety of subsurface formation minerals and organic compounds [3–6]. Over time, the fluids recovered from the well transition from flowback water to natural formation water (commonly termed "produced water"). The quality and quantity of produced water extracted from an O&G formation is spatially and temporally dependent, but typically contains a wide range of total dissolved solids (TDS), hydrocarbons, organic compounds, and dissolved metals [3,5,6].

Historically, most flowback and produced water from unconventional O&G wells are impounded and then trucked off-site for disposal in Class II injection wells [6–8]. However, the availability of sufficient injection well capacity is a potentially restricting aspect in ongoing exploration and development of O&G fields [1]. Although the quantity of Class II injection wells is likely to

^{*} Corresponding author. Tel.: +1 303 273 3402. E-mail address: tcath@mines.edu (T.Y. Cath).

increase in most basins as they mature, the development of new disposal facilities can be complex, requiring significant capital investment and time, and overcoming regulatory barriers. Furthermore, the geology in certain regions such as Pennsylvania (Marcellus shale play) is not conducive for deep well injection, limiting the options for flowback and produced water disposal [1,6,9]. This is especially important considering the potential for seismic activity resulting from the operation of disposal wells. While discharge and dilution of flowback and produced water into municipal wastewater treatment facilities has been attempted, it has been shown to be an inadequate management solution [1.8]. The TDS concentrations that can be accepted by municipal wastewater facilities are limited by regulations, especially those controlling discharge to sensitive aqueous environments. The organic loading of flowback and produced water can also fluctuate significantly, potentially upsetting biological treatment processes and impacting wastewater effluent quality. Therefore, one of the most promising management strategies for these industrial wastewaters is treatment and local reuse for subsequent hydraulic fracturing processes [10,11].

1.2. On-site water reuse

Local and regional reuse of flowback and produced waters can significantly limit the volumes of wastewater sent for deep well injection, thus reducing the environmental impacts and risks associated with regional water trucking [12]. On-site water reuse can also be economically favorable by minimizing exploration expenses through reduced trucking frequency, fresh water procurement for hydraulic fracturing, and wastewater management at deep well injection facilities [13]. However, there are several limiting factors associated with flowback and produced water quality that should be addressed before on-site reuse is considered. Of significant importance is the stability of the chemical constituents and fracturing gels when mixed with reclaimed flowback and produced waters for subsequent hydraulic fracturing operations [1,13,14]. Inorganic precipitates are also of significant concern, specifically precipitation of carbonate and sulfate species in the presence of a variety of dissolved ions (e.g., barium, strontium, and calcium) [1,13–15]. While chemical companies and oil field service providers are continually developing chemical additives that are compatible with high TDS, low quality waters [13,16], the opportunity to generate reuse water of varying qualities is of growing interest. This is especially true for companies interested in both water reuse for hydraulic fracturing and treating and discharging flowback or produced waters to the environment in lieu of deep well injection. A wide variety of technologies can be used for onsite treatment and desalination of flowback and produced waters, including distillation and pressure driven membrane processes [1,2]; however, these technologies are susceptible to premature failure if the feed water is not of suitable quality - traditionally, these wastewaters require multiple upstream pretreatment processes. A multi-step treatment process might limit the efficiency of on-site water treatment, reduce system mobility and modularity, and ultimately become economically unfavorable. Therefore, technologies that employ sustainable driving forces for treatment of high TDS, impaired feed streams and have the capacity to separate a broad range of contaminants are needed for economical treatment of flowback produced water.

1.3. Forward osmosis for treatment of fracturing flowback and produced water

Forward osmosis (FO) is a robust membrane separation technology that can provide superior rejection of a broad range of feed

stream contaminants and TDS, while operating with minimal hydraulic pressure [17]. FO utilizes the chemical potential between a highly concentrated draw solution (e.g., NaCl) and a lower salinity feed solution to drive the permeation of water across a semipermeable membrane. The FO process can achieve solute rejection similar to reverse osmosis (RO), while traditionally avoiding the need for significant upstream pretreatment to mitigate irreversible fouling and premature membrane failure. The FO process has been proposed as a suitable, on-site treatment process for management of flowback and produced waters [2,18]; however, few studies to date have investigated the performance of FO membranes for treatment of these complex feed streams [19–23]. Of those studies, only three were from academia [19.21.23], while the remaining were pilot scale evaluations from industry [20,22]. Hickenbottom et al. [23] first investigated treatment of O&G pit water with a cellulose triacetate (CTA) membrane from Hydration Technology Innovations (Albany, OR (HTI)). Since, Yun et al. [19] and Li et al. [21] have investigated treatment of flowback and produced waters using FO; however, Yun et al. employed synthetic feed solutions, while Li et al. employed a flowback feed stream from O&G exploration that had been chemically and physically pretreated prior to the FO process. Furthermore, both studies used only the CTA membrane manufactured by HTI and employed operating conditions that might misrepresent membrane performance experienced in full-scale FO applications.

1.4. Objectives

The main objective of this study was to investigate the impacts of membrane selection and operating conditions on the performance of FO membranes for desalination of produced water. Specifically, water flux, contaminant rejection, and membrane fouling were evaluated using a combination of standard methodology and system operating conditions analogous to those used in the operation of industrial spiral wound FO membranes. A series of bench-scale experiments were conducted on three polymeric membranes to elucidate the role of initial permeate flux, cross-flow velocity, feed stream turbulence enhancement, and transmembrane hydraulic pressure on fouling of FO membranes operated under extreme feed stream chemistries. Membrane autopsy was also conducted to determine the influence of membrane physiochemical properties on system performance and to interpret the potential molecular level interactions occurring near the membrane-solution interface. The results of this study can be used to determine the applicability of FO operated with spiral wound modules for treatment of complex O&G waste streams without pretreatment.

2. Materials and methods

2.1. FO membranes

Three flat sheet FO membranes were tested. The first membrane was an asymmetric cellulose triacetate (CTA) membrane from Hydration Technology Innovations (HTI) (Albany, OR). This membrane is commercially available and is thoroughly referenced in the literature [17,24–26]. The other two membranes are thin film composite (TFC) polyamide-based membranes also manufactured by HTI. The first TFC membrane is a derivative of a TFC membrane that was studied in a previous investigation (designated TFC1 in this study) [27]. The second TFC membrane is not commercially available and has not been previously described in the literature. The active layer of this membrane was surface-modified by HTI and was designated TFC2 in this study. All experiments were conducted with the membrane active layer

facing the feed solution (FS). The water and solute permeability coefficients (*A* and *B*, respectively) and structural parameter (*S*) of each membrane were determined using methodology presented by Tiraferri et al. [28].

Membrane coupons were soaked in deionized water for 24 h prior to installation in the test cell. No additional membrane wetting techniques were employed. To maintain high quality assurance and control, membrane integrity tests were conducted prior to all experiments. Fouled membranes were removed at the end of each set of experiments and new coupons were installed to minimize performance bias (i.e., water flux, contaminant rejection, and fouling propensity) in subsequent experiments.

2.2. Membrane characterization

2.2.1. Surface roughness and microscopy imaging

Atomic force microscopy (AFM) experiments were performed using an Autoprobe CP atomic force microscope (Park Scientific Instruments, Sunnyvale, CA) coupled with silicon nitride cantilevers and pyramidal tips (VEECO Instruments, Inc., Fremont, CA). Membrane surface morphology was imaged on dry coupons in tapping mode. The roughness of each membrane is reported as average roughness (R_a) and root mean square roughness (R_a).

Membrane fouling was characterized using environmental scanning electron microscopy (ESEM) Quanta 600 (FEI Company, Hillsboro, OR) coupled with energy dispersive x-ray spectroscopy (EDS). Surface and cross-sectional imaging was conducted on each sample analyzed. To view the membrane cross-section, coupons were submerged in liquid nitrogen and cut with a razor blade. Prior to ESEM imaging, samples were sputtered with gold to avoid charging of the non-conductive membrane surface.

2.2.2. Surface charge: streaming potential measurements

Streaming potential analyses were conducted using an electrokinetic analyzer (SurPASS, Anton Paar GmbH, Austria) equipped with an adjustable gap cell which holds two membrane coupons $20~\text{mm} \times 10~\text{mm}$ in size. Streaming potential measurements were conducted at room temperature using 2 mM KCl electrolyte solution, a target ramp pressure of 300 mbar, and gap of $116 \pm 2~\mu\text{m}$ between the membrane coupons. The pH of the electrolyte was adjusted using 0.1 M hydrochloric acid or 0.1 M potassium hydroxide (pH 3–10 for TFC and pH 4–8 for CTA). Streaming potential was measured 4 times at each pH and then averaged to calculate the zeta (ζ) potential using the Helmholtz–Smoluchowski equation [29]

$$\zeta = \frac{dU_{\text{str}}}{dp} \cdot \frac{\eta}{\varepsilon_{\text{r}} \cdot \varepsilon_{0}} \cdot k \tag{1}$$

where $dU_{\rm str}/dp$ is the streaming potential coefficient, $\varepsilon_{\rm r}$ is the relative permittivity of the electrolyte, ε_0 is the vacuum permittivity, η is the electrolyte viscosity, and k is the bulk electrolyte conductivity. The derivation of the Helmholtz–Smoluchowski equation has been presented and discussed in greater detail in previous membrane studies [29,30].

2.2.3. Surface energetics: contact angle measurements

Surface energy parameters of each virgin membrane active layer were estimated using a goniometer (Rame-Hart Inc., Mountain Lakes, NJ). Captive bubble contact angle (θ_c) measurements were conducted under ambient conditions (\sim 20 °C) with deionized water, glycerol (\geq 99%) (Sigma-Aldrich, St. Louis, MO), and diiodomethane (\geq 99%) (Sigma-Aldrich). Steady state contact angle was measured after 1 min of interfacial interaction between the hydrated membrane surface and a 10 μ L air bubble. No less than 10 contact angle measurements were recorded on each membrane coupon. Averaged contact angle measurements were

used to determine the surface energetics of each membrane using the Lifshitz-van der Waals acid-base approach following similar procedures outlined in the literature [31,32]. Estimates of the long-range surface forces (non-polar) and short-range acid-base (polar) forces for each membrane were determined through the extended Young equation [31–34]

$$\left(1 + \cos \theta_c\right) \gamma_l^{TOT} = 2\left(\sqrt{\gamma_s^{LW} \gamma_l^{LW}} + \sqrt{\gamma_s^+ \gamma_l^-} + \sqrt{\gamma_s^+ \gamma_l^-}\right)$$
 (2)

where γ^{TOT} is the total surface tension, γ^{LW} is the Lifshitz-van der Waals parameter, γ^+ is the electron acceptor parameter, and γ^- is the electron donor parameter. The subscripts I and s represent the liquid and solid membrane surface, respectively. Surface tension properties for the three probe liquids were obtained from the literature [35]. The acid-base component and the total surface tension of each membrane's surface were determined using Eqs. (3) and (4), respectively

$$\gamma^{AB} = 2\sqrt{\gamma^+ \gamma^-},\tag{3}$$

$$\gamma^{\text{TOT}} = \gamma^{\text{LW}} + \gamma^{\text{AB}}.\tag{4}$$

The interfacial free energy of adhesion per unit area gives an indication of each membrane's hydrophilicity when submerged in an aqueous solution and can be calculated from the γ^+ , γ^- , and γ^{LW} surface energy components. The total interfacial free energy for each membrane active layer is given by [31,32,35]

$$\Delta G_{132}^{\text{TOT}} = \Delta G_{132}^{\text{AB}} + \Delta G_{132}^{\text{LW}},\tag{5a}$$

$$\Delta G_{132}^{AB} = 2\sqrt{\gamma_3^+} \left(\sqrt{\gamma_1^-} + \sqrt{\gamma_2^-} - \sqrt{\gamma_3^-}\right) + 2\sqrt{\gamma_3^-} \left(\sqrt{\gamma_1^+} + \sqrt{\gamma_2^+} - \sqrt{\gamma_3^+}\right) - 2\sqrt{\gamma_1^+ \gamma_2^-} - 2\sqrt{\gamma_1^- \gamma_2^+},\tag{5b}$$

$$\Delta G_{132}^{\mathrm{LW}} = 2 \bigg(\sqrt{\gamma_{3}^{\mathrm{LW}}} - \sqrt{\gamma_{1}^{\mathrm{LW}}} \bigg) \bigg(\sqrt{\gamma_{2}^{\mathrm{LW}+}} - \sqrt{\gamma_{3}^{\mathrm{LW}}} \bigg). \tag{5c}$$

Surfaces 1 and 2 are assumed as identical membrane active layers; therefore, ΔG_{132}^{TOT} (Eq. (5)) can be simplified to ΔG_{131}^{TOT} , or ΔG_{SWS}^{TOT} , where positive and negative values are indicative of a hydrophilic and hydrophobic membrane surface, respectively [31,32,36].

2.2.4. Surface chemistry: ATR-FTIR spectroscopy

Attenuated Total Reflectance Fourier Transform Infrared Spectroscopy (ATR-FTIR) analysis was conducted in order to characterize the surface chemistry of the membrane coupons. The goal of ATR-FTIR measurements was not to identify individual functional groups of each membrane surface, but to ascertain possible changes to the polymeric surface of the FO membranes after exposure to produced water. Transmittance spectra were measured using a Nicolet IS50 FTIR spectrometer (Thermo Scientific, Madison, WI). The spectrometer was equipped with a built-in ATR (diamond crystal) accessory coupled with a DTGS detector and KBr beam splitter. A gripper device maintained contact between the membrane active layer and the ATR crystal. A background spectrum was measured prior to each membrane analysis and was subtracted from the membrane spectrum using the Omnic analysis software (Thermo Scientific, Madison, WI). Each spectrum was measured using 10 scans at resolution 4 (0.482 cm⁻¹).

2.3. Solution chemistries

The concentrations of major constituents measured in the feed during this study are summarized in Table 1. The feed was a comingled industrial wastewater consisting of produced water influenced by hydraulic fracturing flowback (termed produced

Table 1Average concentrations of major constituents measured in the produced water.

| Constituent | mg/L |
|---|--------|
| рН | 6.9 |
| Total suspended solids | 314 |
| Total organic carbon | 95 |
| Dissolved organic carbon | 70 |
| Total nitrogen | 38 |
| Total carbohydrates (guar) | 50 |
| Alkalinity (as CaCO ₃) | 570 |
| Hardness (as CaCO ₃) | 555 |
| Total dissolved solids (TDS) ^a | 24,646 |
| Fluoride | 37 |
| Chloride | 14,694 |
| Nitrate | 0 |
| Sulfate | 0 |
| Bromide | 88 |
| Barium | 8 |
| Calcium | 1121 |
| Magnesium | 121 |
| Lithium | 6 |
| Potassium | 127 |
| Iron | 79 |
| Manganese | 2 |
| Sodium | 8209 |
| Phosphorous | 5 |
| Silicon | 87 |
| Strontium | 60 |
| Zinc | 1 |
| Nickel | 2 |

^a ΣCations=431.4 meq/L; ΣAnions=-417.5 meq/L.

water in this study) originating from the Niobrara shale formation. The produced water was obtained from an O&G service provider in the Denver-Julesburg basin, located northeast of Denver, CO. To minimize chemical variability in the feed, 210 L of flowback were collected in a single sampling event and stored in a climate-controlled room for the duration of the study. The DS was prepared using ACS grade NaCl (Fisher Scientific, Fair Lawn, NJ).

The cleaning efficiencies of KL7330 (King Lee Technologies, San Diego, CA) and ethylenediamine–tetraacetic acid (EDTA) (Avantor, Central Valley, PA) were investigated in select experiments. KL7330 is a powder cleaner that targets oils, greases, and organic particulates at neutral solution pH, making it suitable for CTA and TFC membrane applications. EDTA was chosen because of its chelating properties, especially for cleaning polymeric membranes fouled by divalent cation–organic compound complexations; the EDTA solution pH was adjusted to pH 11 and pH 7.9 for the TFC and CTA membranes, respectively. The solution strength of both chemicals was 11,000 mg/L following the manufacturer's recommendations.

2.4. Bench-scale FO system

The bench-scale system used in this study was similar to that described in our previous publication [27]; a schematic of the system is provided in Fig. S1 of the Supporting materials. A custom-made membrane test cell with symmetrical flow channels (76 mm \times 255 mm) was employed. Feed and DS flow channel depth was controlled independently using nitrile rubber gaskets in order to incorporate turbulence enhancing spacers. Commercially available tricot and chevron spacers [26] were chosen to mimic the hydrodynamic conditions inside spiral wound membrane elements and were installed in the DS and feed channels, respectively, during select experiments. LabVIEW data acquisition software (National Instruments, Austin, TX) and UE9-Pro DAQ systems (LabJack, Lakewood,

 Table 2

 Summary of bench-scale operating conditions.

| Test set | Experimental condition | Value | Units |
|----------|--------------------------|----------------|-----------|
| A | Feed cross-flow velocity | 0.20 | m/s |
| | DS cross-flow velocity | 0.20 | m/s |
| | Transmembrane pressure | < 0.07 (1) | bar (psi) |
| | DS spacer/feed spacer | tricot/NA | NA |
| В | Feed cross-flow velocity | 0.20 | m/s |
| | DS cross-flow velocity | 0.20 | m/s |
| | Transmembrane pressure | < 0.07 (1) | bar (psi) |
| | DS spacer/feed spacer | tricot/chevron | NA |
| С | Feed cross-flow velocity | 0.30 | m/s |
| | DS cross-flow velocity | 0.10 | m/s |
| | Transmembrane pressure | 0.27 (4) | bar (psi) |
| | DS spacer/feed spacer | tricot/chevron | NA |
| D | Feed cross-flow velocity | 0.30 | m/s |
| | DS cross-flow velocity | 0.10 | m/s |
| | Transmembrane pressure | 2.76 (40) | bar (psi) |
| | DS spacer/feed spacer | tricot/chevron | NA |

CO) were used to control experimental test conditions (i.e., solution temperature, feed volume, and DS concentration) and to collect experimental data (i.e., permeate volume, DS and feed conductivity).

2.5. Experimental procedures

All tests were conducted with 1 L (initial volume) DS (1 M NaCl) and 3 L of produced water FS at constant temperature ($20\pm0.5\,^{\circ}$ C). The feed volume and DS concentration were held constant by intermittent dosing of deionized water into the feed tank and concentrated NaCl stock solution ($300\,\text{g/L}$) into the DS tank. Batch experiments with hydrodynamic conditions similar to recently published standard methodology and conditions analogous to those in spiral wound FO elements were performed during four separate test sets (Table 2).

For each set of experiments, a new membrane was installed in the membrane cell and tested with a produced water feed for 24 h. After 24 h, the system was stopped and the draw solution was replaced with deionized water, leaving the produced water in the feed hydraulic system in order to induce an osmotic backwash. In osmotic backwashing the direction of water permeation is reversed, thus removing foulants that have accumulated at the surface of the membrane [37,38]. The fouled membrane was osmotically backwashed for 30 min at 0.2 m/s cross-flow velocity in both flow channels and 0.07 bar transmembrane pressure (TMP) in favor of the feed. Following osmotic backwashing, the feed and DS were replaced with new produced water and NaCl brine and the membrane fouling test was resumed for an additional 24 h. Fouled membranes were osmotically backwashed once more and removed from the test cell for autopsy; half of the coupon was stored wet at 5 °C, while the other half was dried in a desiccator.

2.5.1. Baseline membrane performance

Hydrodynamic conditions similar to recently published standard methodology were used during test set A [27]. This test set was conducted with 0.2 m/s cross-flow velocity in both flow channels to minimize TMP across the membrane (< 0.07 bar in favor of the feed). No spacer was installed in the feed channel; however, a triple layered tricot spacer was used in the DS channel to provide mechanical support to the membrane and maintain a uniform flow channel. DS spacers were also used in test set A to ensure that changes in membrane performance observed in later test sets were independent of the DS spacer [39]. Results from test set A provided a baseline for comparing disparities in membrane

fouling due to differences in membrane surface chemistry and physiochemical properties. The baseline results also served as a benchmark for comparing changes in membrane performance when operating under physical and hydrodynamic conditions similar to those used in spiral wound FO elements.

2.5.2. Membrane performance under spiral wound operating conditions

The physical and hydrodynamic operating conditions shown in Table 2 were varied stepwise during test sets B through D. The goal was to systematically elucidate membrane performance and fouling under conditions similar to those expected in spiral wound FO elements. Experiments from test set B were conducted with the same cross-flow velocities and TMP as those in test set A; however, a chevron spacer was installed in the feed channel to investigate changes in membrane performance and permeation drag forces in the presence of a feed turbulence enhancer. Experiments in test set C were conducted with the same spacers as in test set B, but the feed cross-flow velocity was increased from 0.2 m/s to 0.3 m/s and TMP was increased from 0.07 bar to 0.27 bar. Operating conditions in test set C were in agreement with those suggested by HTI in a previous study by Ren et al. [40]. These operating conditions were used to mimic conditions in spiral wound FO elements operated at the outlet of commercial FO pressure vessels. Experiments in test set D were conducted with the same spacers and cross-flow velocities as those in test set C. However, the TMP was increased from 0.27 bar to 2.76 bar to simulate the pressure conditions inside spiral wound elements operated near the inlet of a commercial FO pressure vessel with multiple elements operated in series [27].

2.5.3. Chemical cleaning

The efficiency of chemically enhanced osmotic backwashing using KL7330 and EDTA was investigated in an additional set of experiments for an extended duration. Experiments under conditions of test set D were repeated on select membranes and the test duration was increased from 48 h to 96 h. After every 24 h of membrane fouling test, the feed and DS were replaced with 1 L of cleaning solution and 1 L of deionized water, respectively. The membrane was chemically cleaned for 30 minutes using the same operating conditions employed during osmotic backwashing. After chemical cleaning the feed and DS were replaced with new produced water and NaCl brine and membrane fouling test was resumed for another 24 h, after which the cleaning procedure was repeated. After 96 h of membrane testing, the coupon was chemically cleaned one more time and removed for autopsy. A new membrane coupon was used when investigating each chemical cleaning solution. It should be noted that membrane cleaning was not optimized in this study. The goal was to establish the effectiveness of traditional osmotic backwashing versus chemical cleaning after FO treatment of produced water to provide insight for future studies.

2.6. Sampling and analytical methods

Cation concentrations were analyzed using inductively coupled plasma atomic emission spectroscopy (ICP-AES) (Optima 5400, PerkinElmer, Fremont, CA) according to the Standard Method 3120 B. Samples were diluted as necessary to bring sodium concentrations below 500 mg/L and acidified with HNO₃ to below pH 2. Feed samples were also filtered through a $0.45\,\mu m$ filter to remove suspended solids prior to analysis. Anion concentrations were analyzed using ion chromatography (IC) (ICS-90, Dionex, Sunnyvale, CA) according to the Standard Method 4110 B. All samples were diluted as necessary to bring chloride concentrations below 500 mg/L and feed samples were filtered through a 0.45 um filter to remove suspended solids prior to analysis. A carbon analyzer (Shimadzu TOC-L, Columbia, MD) using the combustion catalytic oxidation method was employed to determine total organic carbon (TOC), dissolved organic carbon (DOC), and total nitrogen (TN) concentrations. 3-D fluorescence spectroscopy analyses were performed on DS samples using a spectrofluorometer (Aqualog, HORIBA Scientific, Edison, NJ). Fluorescence spectroscopy of samples at 20 °C were analyzed for emission wavelengths between 300 nm and 600 nm and excitation wavelengths between 240 nm and 480 nm. EEMs from each membrane were normalized by DOC concentration (2 mg/L) to better differentiate between DOC fractions that preferentially permeated through each membrane.

Feed samples were also analyzed for hardness, alkalinity, and total carbohydrate concentration. Hardness was calculated from analytical results provided by ICP-AES. Alkalinity was determined via titration using sulfuric acid and HACH method 8203. The anthrone method [41] was used to determine total carbohydrate concentration in the produced water. It was assumed that any concentration of carbohydrates in the feed was attributed to guar gum that is commonly cross-linked and used as a gelling agent during hydraulic fracturing [42].

3. Results and discussion

3.1. Membrane properties

The measured physiochemical properties of each virgin FO membrane used in this study are summarized in Table 3. CTA exhibited the lowest pure water permeability, solute permeability, and structural parameter of the three membranes tested. TFC1 showed significantly greater pure water permeability than CTA, but also exhibited a much larger solute permeability and structural parameter. Similar to TFC1, the pure water permeability of TFC2 exceeded that of CTA; however, the solute permeability of TFC2 was much lower than that of TFC1 and its structural parameter was nearly identical to that of the CTA membrane.

The surface energy data shows that all three membranes have similarly high Lifshitz-van der Waals components (γ^{LW}) and low

Table 3Membrane physical and chemical properties.

| Membrane | Pure water permeability (A) (L m ⁻² h ⁻¹ bar ⁻¹) ^a | Salt permeability (B) $(L m^{-2} h^{-1})^a$ | Structural parameter (S) (µm) ^a | γ ^{LW} (mJ/m ²) | γ ⁺ (mJ/m ²) | γ̄ (mJ/m²) | γ ^{AB} (mJ/m ²) | γ ^{TOT} (mJ/m ²) | ΔG_{SWS} (mJ/m ²) | Z (mV) ^b | Roughness R _a /R _q (nm) |
|--------------|---|---|--|---|--|---------------|--------------------------------------|---------------------------------------|---------------------------------------|------------------------|---|
| CTA | 0.271 | 0.104 | 479 | 37.1 | 1.3 | 27.6 | 11.8 | 48.9 | -0.9 | | 23.4/29.5 |
| TFC1 TFC2 | 1.470 1.040 | 0.622 0.230 | 742 483 | 34.2 38.8 | 1.1 2.2 | 57.0 33.6 | 15.7 17.3 | 49.9 56.1 | 37.4 5.8 | -24.1 -9.0 | 23.1/28.6 10.4/13.6 |

^a Determination of transport and structural parameters of FO membranes was achieved by methods proposed by Tiraferri et al. [28]. Four different draw solution concentrations were employed during membrane characterization. The maximum observed coefficient of variation between J_w/J_s ratios measured in the various stages was 8.7%. The minimum coefficients of determination calculated by the non-linear fitting procedure for R^2 (J_w) and R^2 (J_s) were 0.97 and 0.97, respectively.

^b 2 mM KCl electrolyte at pH 7

electron acceptor components $(\gamma^+).$ The values for $\gamma^{\rm LW}$ and γ^+ increased in the order TFC2 > CTA > TFC1. For each membrane, the electron donor component (γ^{-}) was significantly greater than the electron acceptor component ($\gamma^-/\gamma^+ \ge 15.3$), indicating a high degree of monopolarity for each polymeric surface. These results are consistent with the negative zeta potential values that were calculated for all three membranes. The γ^- values are also in agreement with previous studies that characterized a variety of polymeric membranes as having high electron donor monopolarity [31,33,34]. The γ^- component of TFC1 was the highest of all three membranes, while that of TFC2 was only slightly higher than that of the CTA membrane. These values translate into moderate acid-base components (γ^{AB}) that are approximately 50% lower than the respective γ^{LW} component of each membrane and increased in the order TFC2 > TFC1 > CTA. The magnitude of the γ^{AB} value for each membrane, in relation to its γ^{LW} value, was used to calculate the free energy of cohesion (ΔG_{SWS}) (Eq. (5a)) and estimate the membrane's hydrophobicity/hydrophilicity. Values of ΔG_{SWS} show that TFC1 is strongly hydrophilic, the surface of TFC2 can be considered slightly hydrophilic, and the surface of CTA can be considered neither hydrophilic nor hydrophobic. In general, the surface roughness of CTA and TFC1 are comparable while that of TFC2 is substantially lower.

3.2. FO membrane fouling by O&G produced water: effects of membrane selection

Decline in water flux for each of the three membranes during test set A is presented in Fig. 1 as a function of cumulative permeate volume. The water flux (J_w) of each membrane is normalized to its initial water flux (J_{w0}) recorded at the beginning of the experiment. The normalized water flux shows a distinct, two-stage fouling process separated by the osmotic backwashing. During the initial fouling of the virgin membranes, water flux declines exponentially followed by a gradual transition into near linear flux decline. Constant water flux was not reached before the membranes were osmotically backwashed. Less than 50% of the original water flux was recovered for the three membranes after osmotic backwashing, indicating potential irreversible fouling. After osmotic backwashing, a near linear flux decline was observed for the three membranes. The overall loss in membrane performance due to fouling during test set A was least for CTA, followed by TFC1 and TFC2.

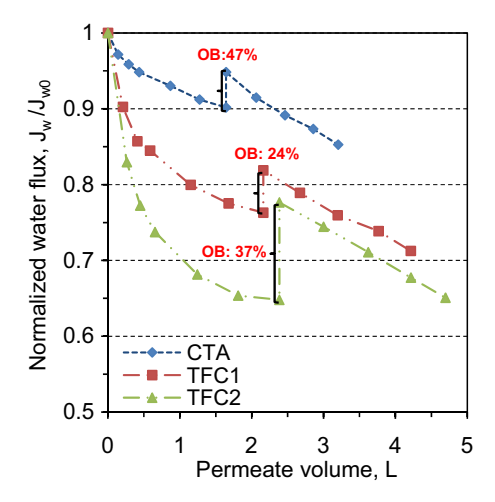


Fig. 1. Normalized water flux for CTA, TFC1, and TFC2 during test set A employing operating conditions described in Table 2. Water flux was normalized to the initial water flux for each membrane, independently. Osmotic backwashing (OB) was conducted after 24 h of membrane fouling during each test set. The initial water flux (J_{w0}) was 3.9 LMH, 5.7 LMH, and 7.2 LMH for CTA, TFC1, and TFC2, respectively.

It is evident that membrane fouling and flux decline occurring before osmotic backwashing is directly proportional to initial water flux and potentially due to permeation drag force of foulants towards the membrane surface. The initial water flux of TFC2 was highest during test set A (7.2 LMH), exceeding that of TFC1 (5.7 LMH) and CTA (3.9 LMH). Note the lower water flux of each membrane due to the high salinity of the feed (\sim 25,000 mg/L TDS $(\sim 0.43 \text{ M}))$ relative to the 1 M NaCl DS. Similar findings were presented in recent publications, where the relationship between membrane fouling and initial water flux was investigated [43–45]. Although each membrane exhibits unique physiochemical surface properties (Table 3), a clear relationship between flux decline and membrane hydrophobicity and surface roughness could not be established. This is despite the overwhelming evidence supporting the correlation between membrane surface properties and flux decline under mild fouling conditions in recent publications [45-51]. Increased fouling due to electrostatic charge shielding of the membrane surface has also been previously proposed [52]; however, similar zeta potentials and thus electrostatic attractionrepulsion forces are expected for the three membranes at high ionic strength based on findings presented in our recent study [53]. It is important to note that the water flux of TFC2 was higher than TFC1 during test set A, despite having a slightly lower pure water permeability coefficient (Table 3). Lower than expected TFC1 water flux was attributed to greater internal concentration polarization resulting from its high structural parameter, thus hindering osmotic driving force [44,54].

During osmotic backwashing, 47% of the loss in water flux was recovered for CTA, followed by 24% for TFC1 and 37% for TFC2. Based on the above results and direct observation of the membrane surface, we infer that the osmotic backwashing removed the majority of the loosely bound foulants near the surface of the complex cake layer, while the foulants sorbed to the membrane surface were not entirely removed. Higher cleaning efficiency for CTA was indeed expected due to lower permeation drag during filtration and the relatively low permeate volume (1.6 L) compared to the TFC membranes. Flux recovery for TFC1 was much lower than CTA due to greater foulant deposition during filtration and higher permeation drag towards the membrane surface. It is also possible that this higher permeation drag force increased the compaction of foulants in the feed stream onto the TFC1 membrane surface, especially into the nano-scale valleys of the rough active layer. Interestingly, flux recovery for TFC2 was only 10% lower than CTA despite exhibiting the highest permeation drag force and achieving the greatest filtration volume. This flux recovery is attributed to the relatively smooth surface of TFC2, which is over 50% less rough than TFC1 and CTA. It is well documented that low surface roughness can minimize irreversible fouling and increase the DLVO surface energetics of the membrane surface [45,46,51,55].

After osmotic backwashing, flux decline was near linear regardless of membrane type. This indicates that long-term fouling and flux decline when treating produced water is dominated by foulant–foulant interactions near the surface of the cake layer. Similar conclusions were drawn in previous studies that investigated organic fouling and cleaning of FO membranes [46,56].

3.3. Effects of operating conditions on FO membrane performance

Normalized water flux as a function of time is shown in Fig. 2 for CTA, TFC1, and TFC2 under the four different operating conditions tested (Table 2). In general, flux decline before osmotic backwashing correlated well with initial water flux. After osmotic backwashing, flux decline appeared to be controlled by foulant-foulant interactions based on the near linear decline in water flux and lack of exponential flux decline observed when employing

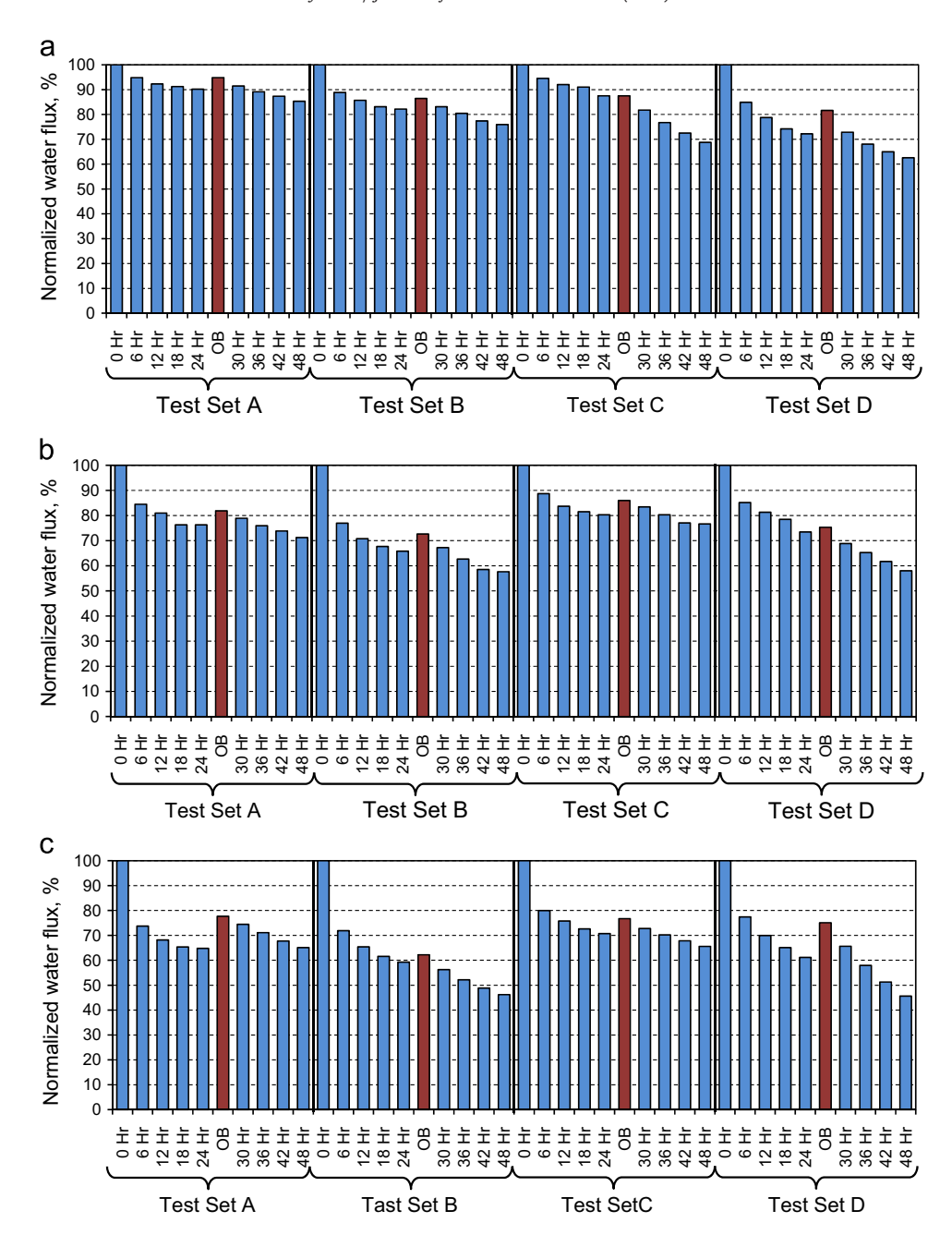


Fig. 2. Normalized water flux for the (a) CTA, (b) TFC1, and (c) TFC2 membrane fouling tests. Test sets indicate intervals of different operating conditions during the bench-scale study and are defined in Table 2. Water flux was normalized to the initial flux for each test set, independently. Osmotic backwashing (OB) was conducted after 24 h of membrane fouling during each test set. The average initial water flux for each membrane was 4.3 ± 0.3 LMH for CTA, 7.4 ± 1.4 LMH for TFC1, and 7.2 ± 0.7 LMH for TFC2.

virgin membranes; however, the rate of flux decline was impacted by changes in hydrodynamic conditions in each test set. Flux recovery after osmotic backwashing was similar for all test sets and there was no clear correlation between changes in hydrodynamic test conditions and osmotic backwashing cleaning efficiency.

A chevron spacer was installed in the feed channel during experiments in test set B; all other operating conditions were the same to those employed in test set A. The presence of the chevron spacer exacerbated membrane fouling compared to baseline results obtained in test set A. After 24 h of testing, water flux had declined by 20%, 34%, and 40% for CTA, TFC1, and TFC2, respectively. Direct observation of the membrane surface (Fig. 3) revealed that foulant deposition was severe at the contact points between the spacer and the membrane surface, which likely reduced surface area for water permeation and increased the effects of cake enhanced concentration polarization [57], which reduced the effective osmotic driving

force across the membranes. These findings are supported by Park and Kim [39], who demonstrated the effects of feed spacers on concentration polarization near the spacer–membrane interface in FO when employing feed streams with variable concentrations of NaCl. Water flux continued to decline after osmotic backwashing in test set B and the final water flux of each membrane was lower than that observed in test set A after 48 h of operation.

Experiments in test set C were conducted at higher feed cross-flow velocity, and thus higher tangential shear force, to minimize foulant deposition and reduce external concentration polarization. The operating conditions employed in test set C also simulate the hydrodynamic conditions in the last spiral wound FO elements of a multi-element commercial pressure vessel. Membrane fouling and flux decline were reduced for each membrane compared to test set A and test set B. After 24 h of testing, water flux had declined by 13%, 20%, and 30% for CTA, TFC1, and TFC2, respectively. Again, flux



Fig. 3. Images of virgin and fouled CTA, TFC1, and TFC2 membrane samples. Fouled coupons are from membranes used under test set A and test set B conditions.

recovery after osmotic backwashing was similar to that of all previous test sets. Membrane performance observed during test set C indicate that increased cross-flow velocity could minimize foulant deposition and water flux decline over time, despite increased fouling propensity and irreversible fouling at the feed membrane–spacer interface.

The effects of increased hydraulic pressure in the feed channel were also investigated at high cross-flow velocity, similar to that employed in test set C. Membrane fouling and water flux decline in test set D were higher than those observed in all other test sets. No significant difference in osmotic backwashing efficiency was observed. These results indicate that cake layer compaction due to hydraulic pressure may play a major role in controlling water flux in FO fouling, especially in spiral wound membrane elements employed in full-scale systems. It is also likely that increased cake layer compaction exacerbated the effects of cake enhanced CP, due to the hindered convection and diffusion of ions (resulting from reverse solute diffusion) away from the active layer and through the foulant layer. It is important to note that the magnitude of TMP used in this study has negligible impacts on water flux of FO membranes [27]. Therefore, changes in water flux are only due to foulant deposition and cake layer compaction on the membrane surface.

Results from the current study suggest that during treatment of produced water with spiral wound modules, FO membrane fouling could be exacerbated by the presence of feed spacers. This raises questions regarding use of spiral wound FO elements for treatment of complex feed streams with minimal pretreatment [2], especially in light of results from a recent study where activated sludge was treated with plate-and-frame FO modules for over 120 days with no cleaning and minimal fouling [58]. In spiral wound FO modules, membrane performance can be increased and fouling minimized by increasing cross-flow velocity; however, this can increase the energy demand of the FO system significantly. For example, in a recent pilot scale study in the Haynesville Basin [2] the energy demand of the FO system was approximately 15 – kWh/m³ when operated under conditions similar to this study (test sets C and D). This value exceeds the energy demand of traditional seawater reverse osmosis by nearly 4 times. It is important to note that this energy demand is likely to decrease substantially (from 15 kWh/m³ to 5 kWh/m³) if the feed spacer thickness is minimized (100-30 mil) due to significantly lower pumping requirements to maintain adequate cross-flow velocity in the membrane module; however, feed pretreatment is required in O&G applications if feed spacer thickness is reduced. At \$0.10 kWh, 15 kWh/m³ translates to \$0.24 cost of energy for treatment of one barrel (42 US gallons=159 L) of produced water. This is a very low

O&M (energy is > 75% of O&M) for treatment of produced water, especially given the high quality permeate that is generated with no pretreatment of the feed water (see Section 3.4).

3.4. Contaminant rejection by FO membranes

3.4.1. Rejection of inorganic solutes

The rejection of dissolved inorganic ions during test set A and test set D for the three membranes is shown in Fig. 4. These results represent solute rejection during experiments that exhibited the least (A) and most (D) membrane fouling and flux decline. Greater than 94% rejection of cations by the CTA membrane was observed in both test sets (Fig. 4a); the concentrations of feed anions (i.e., bromide, fluoride, sulfate, nitrate, and phosphate) in the DS were below detection limit throughout the study. Comparable cation rejection under the different testing conditions indicates that the diffusion of each analyte was largely independent of valence, molecular weight, and hydration radius. The rejection of divalent cations by CTA was slightly lower than that observed in previous studies [23,27,59]. This is likely due to cake enhanced CP resulting from the complexation of divalent cations with DOC at the membrane surface [47]. ATR-FTIR transmittance measurements of the fouled membrane surfaces indicated an overwhelming presence of calcium carbonate with traces of oil residues (> 93.5% compound match to Omnic software library (Fig. S2 in the Supporting materials)). The zeta potential of each fouled membrane was also 10-20 mV more negative than virgin samples (at pH 7), further supporting the likelihood of cake enhanced CP resulting from divalent cation-DOC complexation at the membrane surface (Fig. S2 in the Supporting materials). Similar findings were presented by Childress et al. [29], while investigating the impacts of humic acid in the presence of divalent cations on membrane zeta potential. Membrane scaling was also probable due to high carbonate concentrations in the feed, which would be exacerbated near the membrane surface. Cake enhanced CP and membrane scaling increased the solute concentration at the membrane boundary layer and thus the driving force for diffusive-based transport of ions into the DS. Higher ion transport (lower rejection) was measured during test set D, which was attributed to lower water recovery (compared to test set A) and severe cake enhanced CP due to cake layer compaction at high TMP.

Ion rejection by the polyamide TFC1 membrane (Fig. 4b) was lower than that of the CTA membrane. Monovalent cation rejection increased with molecular weight and hydration radius. Divalent cation rejection was greater than 95% and comparable for all solutes regardless of valence and molecular weight. Similar

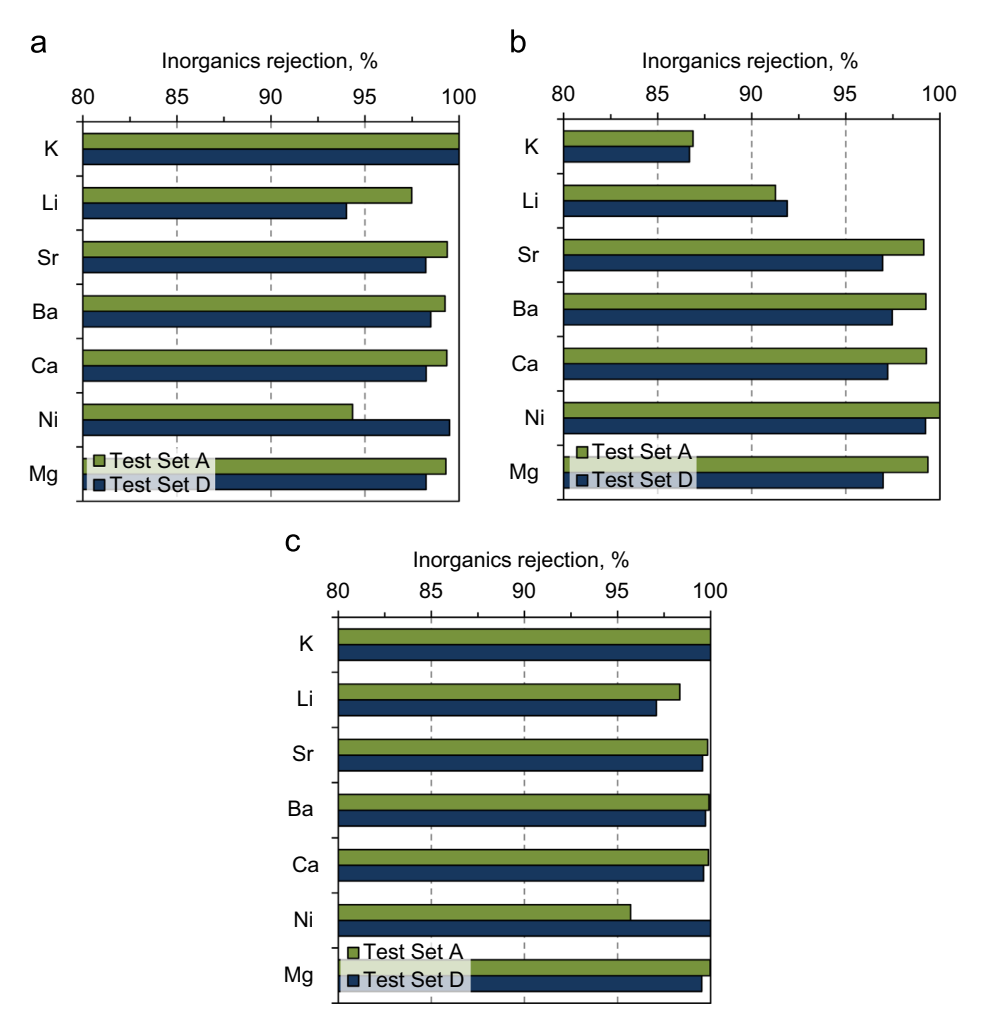


Fig. 4. Rejection of dissolved ions by the (a) CTA, (b) TFC1, and (c) TFC2 membranes during test sets A and D. Operating conditions for each test set are shown in Table 2.

to CTA, rejection of divalent cations was lower than anticipated due to cake enhanced concentration polarization and membrane scaling. Lower cation rejection by TFC1 was also expected due to electrostatic attraction to the functionalized polymer surface, regardless of ionic strength [53]. Contrary to the results observed with TFC1, cation rejection measured for TFC2 (Fig. 4c) was the highest throughout the study despite severe membrane fouling; at least 96% rejection of cations was measured in both test sets. While the physiochemical properties of TFC2 are similar to that of CTA (Table 2), the membrane zeta potential of TFC2 is near neutral and might result in lower electrostatic attraction of feed cations to the membrane surface and minimize CP. Similar to CTA, cation rejection by both polyamide TFC membranes was lower during test set D due to lower water recovery (compared to test set A) and severe cake enhanced concentration polarization.

3.4.2. Rejection of dissolved organic carbon and total nitrogen

The rejection of DOC and total nitrogen (TN) by the three membranes during test sets A and D are shown in Fig. 5. The rejection of DOC was in agreement with trends observed with inorganic ion rejection. TFC2 exhibited the highest rejection of DOC, followed by CTA and then TFC1. The lowest DOC rejection observed throughout the study was 93% by TFC1, while the highest rejection was nearly 98% for TFC2. DOC rejection was similar for all membranes tested regardless of operating conditions; however, slightly higher DOC rejection was measured (Fig. 5a) when increased membrane fouling was observed (Fig. 1). These results

suggest that cake layer formation on the membrane surface effectively shields the active layer and increases the sorption capacity for additional contaminants, while reducing the mass transport capacity. Increased DOC rejection also shifts the membrane zeta potential more negative [29], increasing the electrostatic attraction of cations near the membrane surface and thereby increasing the concentration gradient across the membrane boundary layer. Therefore, lower cation rejection due to CP (Fig. 4) is exacerbated by increased electrostatic attraction and correlates well with increased DOC concentration at the membrane surface.

All membranes in the study poorly rejected TN present in the produced water, and no obvious correlation with membrane fouling was observed. TN rejection ranged from 85% to 89% for CTA and from 59% to 67% for TFC1. The performance of TFC2 was more consistent and TN rejection was approximately 84% during both test sets. Although the mass transport of TN could not be correlated with molecular weight and hydration radius, it appears that the order of TN rejection by each membrane was similar to that observed for inorganic ion rejection (CTA \approx TFC2 > TFC1).

Fluorescence spectrophotometry was employed to qualitatively characterize the composition of dissolved organic compounds that diffused across the different polymeric membranes. Excitation-emission (EEM) plots of the draw solutions from the end of test set D are shown in Fig. 6. A list of peaks identified in this study and observed in previous publications is summarized in Table 4. No peaks were observed in the initial draw solution (not shown) and the system was operated at constant DS concentration. Therefore,

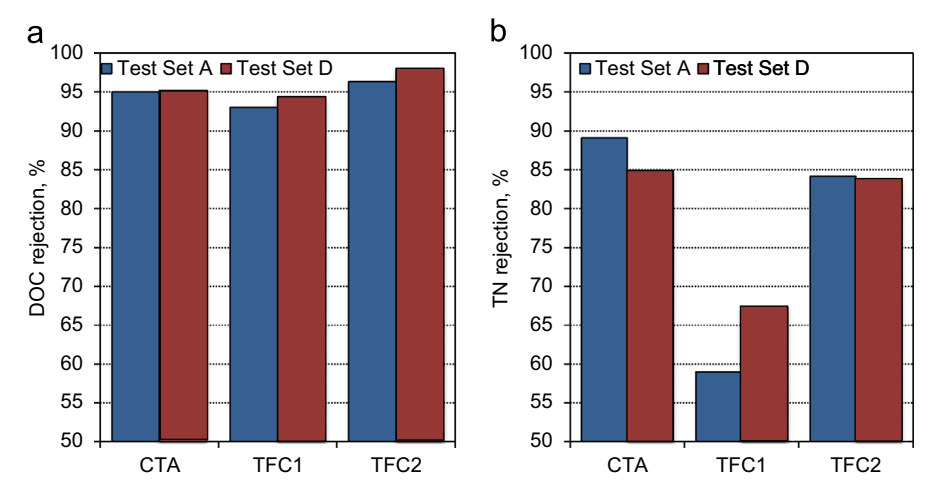


Fig. 5. Rejection of (a) dissolved organic carbon (DOC) and (b) total nitrogen by the CTA, TFC1, and TFC2 membranes during test sets A and D. Operating conditions for the test set are summarized in Table 2.

the peaks shown in DS samples from the end of the experiment are due to the diffusion of organic compounds across the membrane and subsequent accumulation in the DS tank.

Marine humic-like organic compounds (Table 4) were present in the DS after experiments with the CTA membrane (Fig. 6a), but no fulvic-like organic compounds were identified. Visible humiclike and soil fulvic-like organic compounds were present in the TFC1 DS (Fig. 6b) and little influence of marine humic-like organic compounds was detected. The difference in organic composition between the CTA and TFC1 final DS indicates that preferential diffusion of different organic compounds might be a function of polymer chemistry and supports the similar observations reported for the rejection of TN (some of which is definitely organic nitrogen). Interestingly, the characteristics of the organic compounds detected in the TFC2 DS (Fig. 6c) were broad and similar to both the CTA and TFC1 membrane, despite its superior rejection. A broad peak indicative of marine humic-like and visible humic-like organic compounds was identified in addition to a soil fulvic-like organic peak. Fluorescence peaks shown in Fig. 6 are also similar to those of several common polycyclic aromatic hydrocarbons previously investigated by Ferretto et al. [60]; however, several of these peaks overlap with different organic compounds observed in previous studies [61-64]. While the EEMs obtained in our study support conclusions regarding the preferential diffusion of organic compounds based on membrane polymer chemistry, they also show that a key focal point in future studies must be the advancing of analytical capabilities for characterizing the DOC in produced water to better understand the preferential diffusion of organic compounds across different membranes.

3.5. Effects of chemical cleaning on membrane performance

The long term performance and effects of chemical cleaning of CTA and TFC2 are shown in Fig. 7. Each membrane was tested for 24 h with produced water feed and then chemically cleaned using EDTA or KL7330 for 30 min. After chemical cleaning, the membranes were tested for an additional 24 h with produced water feed to compare between the fouling propensity of virgin and chemically cleaned membranes; this process was repeated three times (total of 96 h). The water flux of each membrane is normalized to the initial water flux recorded at the beginning of the experiment.

In general, the normalized water flux data is similar to results shown for test set D in Fig. 2. During the initial fouling of the virgin CTA membrane, the water flux declines exponentially, followed by a gradual transition into near linear flux decline. During the initial

fouling of the virgin TFC2 membrane, the water flux declines exponentially throughout the first 24 h of testing. Steady state water flux was never reached before each membrane was chemically cleaned. Water flux was consistently returned to near 90% of the initial flux (or greater) for the two membranes, resulting in significantly less irreversible fouling compared to osmotic backwashing cleaning. During subsequent fouling of each membrane, a similar decline in water flux was observed for each membrane, indicating that chemical cleaning effectively cleaned the membranes to near virgin conditions. Similar to results above (Figs. 1 and 2), the decline in water flux was greatest for the TFC2 membrane, despite effective chemical cleaning every 24 h.

After chemical cleaning, water flux through CTA recovered by approximately 78% and 72% for the KL7330 and EDTA, respectively (Fig. 7a). The cleaning performance of EDTA remained nearly constant across all three cleaning events; however, the cleaning efficiency of KL7330 gradually declined and flux recovery was only 53% after the last cleaning event. Based on the above results and direct observation of the membrane surface, we infer that KL7330 is suitable for targeting the loosely bound organic foulants near the surface of the complex cake layer, but inefficient at addressing divalent-organic compound complexations and scaling at the CTA membrane interface. These findings are supported by the change in CTA membrane fouling during each subsequent fouling experiment. The exponential flux decline observed early in the experiments changed to near linear flux decline by the end of the study, indicating a gradual shift from fouling dominated by membrane-foulant interactions to foulant-foulant interactions. Furthermore, these findings are also supported by the consistent cleaning efficiency of EDTA, which specifically targets divalent-organic compound complexations in the cake layer. Water flux through the TFC2 membrane recovered by approximately 75% and 73% for the KL7330 and EDTA, respectively (Fig. 7b). Despite the highest permeation drag force and filtration volume of the two membranes, the cleaning efficiency of TFC2 was comparable to CTA. Interestingly, even the cleaning performance of KL7330 for TFC2 remained consistent throughout the entire experiment and did not decline (compared to CTA). Therefore, it is likely that the extremely smooth surface of TFC2 enabled greater chemical cleaning efficiency of the membrane. These findings raise important questions regarding the economic tradeoffs between operating spiral wound FO systems with lower flux CTA membranes (resulting in lower fouling propensity) or with higher flux (and thus higher fouling rate) TFC membranes with potentially equal or superior cleaning properties to CTA.

After the final chemical cleaning event, each membrane coupon was removed for autopsy (ESEM coupled with EDS, ATR-FTIR, and

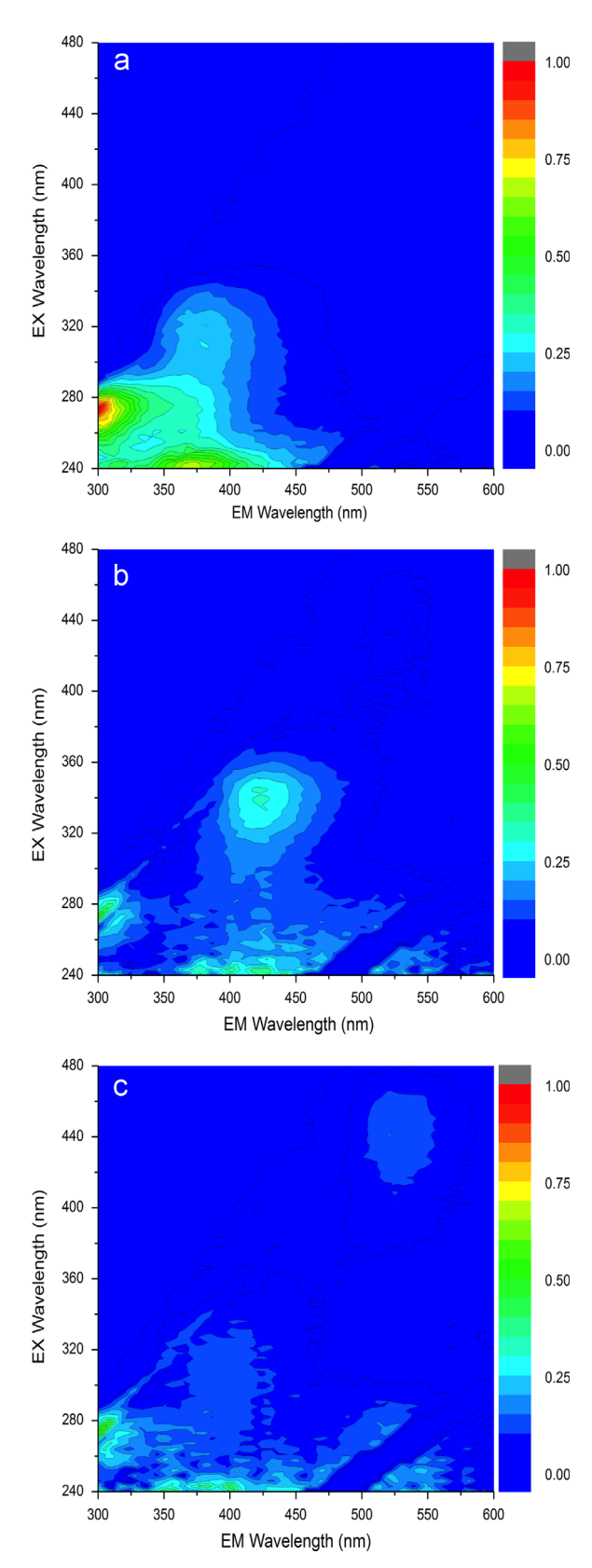


Fig. 6. Comparison of draw solution EEMs at the end of test set D for (a) CTA, (b) TFC1, and (c) TFC2. All EEMs intensities are normalized to a draw solution DOC concentration of 2.0 mg/L.

zeta potential) to investigate membrane robustness and identify any possible changes to the membrane surface. Representative ESEM micrograph and EDS spectra are shown in Fig. 8 for TFC2 chemically cleaned with EDTA. In general, the chemical cleaning process

successfully removed most foulants from the membrane surfaces that were not in contact with the chevron spacer (Fig. 8a and b). At points where the chevron spacer contacted the active layer, a significant cake layer was formed on the membrane surface. Neither chemical was

 Table 4

 Previously identified spectra positions of the fluorescence maxima of dissolved organic matter and select PAHs.

| Description | Emission max (nm) | Excitation max (nm) | Ref. | |
|---------------------------|-------------------|---------------------|---------|--|
| Marine humic-like 370–410 | | 290-310 | [63,64] | |
| Visible humic-like | 420-460 | 320-360 | [63,64] | |
| Soil fulvic acid-like | 521 | 455 | [63,64] | |
| Fluorene | 310 | 260 | [60] | |
| Phenanthrene | 366 | 250 | [60] | |
| Anthracene | 382 | 245 | [60] | |
| | 402 | 245 | | |
| Pyrene | 374 | 240 | [60] | |
| - | 392 | 240 | | |

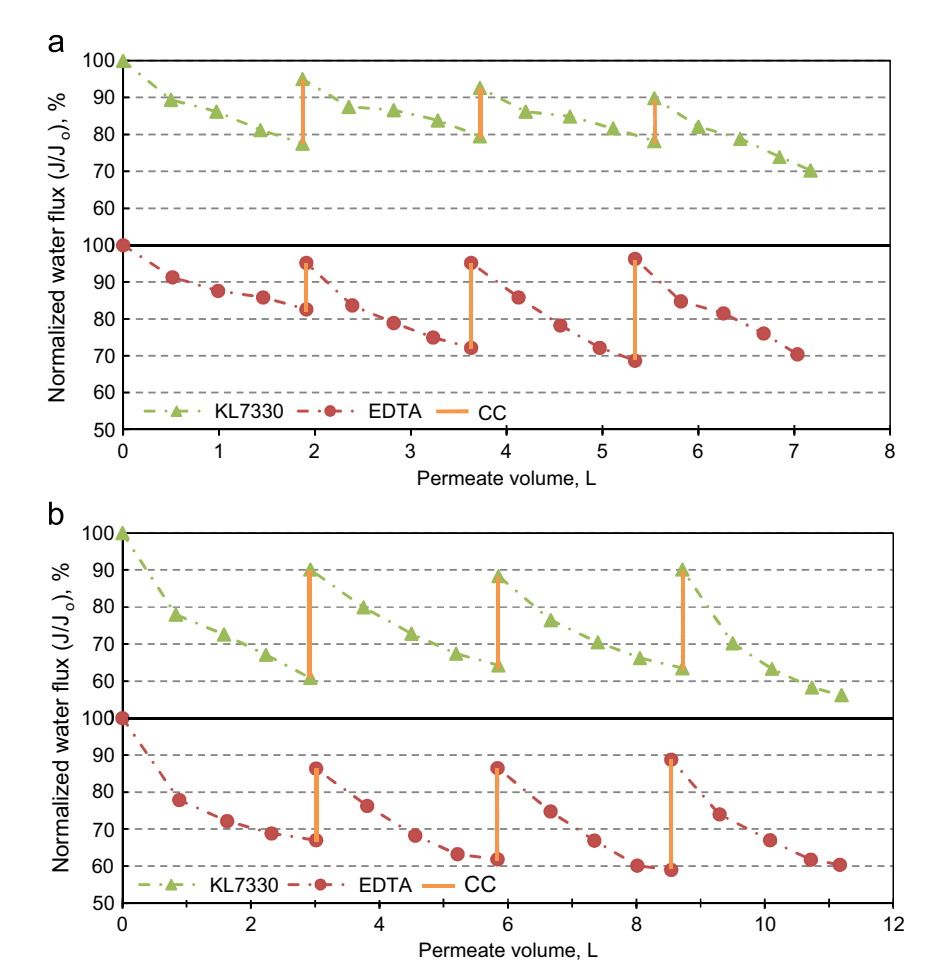


Fig. 7. Normalized water flux data for (a) the CTA membrane chemically cleaned with KL7330 and EDTA and (b) the TFC2 membrane chemically cleaned with KL7330 and EDTA. Fouling tests were conducted using experimental conditions outlined in test set D (Table 2). Water flux was normalized to the initial flux for each experiment. Chemically cleaning (CC) was conducted for 30 min after every 24 h of continuous membrane testing with produced water feed. The average initial water flux was 4.6 ± 0.0 LMH for the CTA and 8.6 ± 0.1 LMH for the TFC2.

effective at removing this irreversible fouling layer from the membrane–spacer interface, thus providing a nucleation site for subsequent foulant deposition and attachment. EDS spectra (Fig. 8c) taken from multiple areas of the cake layer revealed a significant presence of iron, barium, and calcium precipitates, which is consistent with the scaling tendencies predicted by OLI for this particular produced water. These findings were consisted for both membranes, regardless of chemical used.

ATR-FTIR transmittance spectra and zeta potential measurements are presented in Fig. 9 for both membranes. Virgin coupons were analyzed in addition to coupons fouled and chemically cleaned to identify possible changes to each FO membrane after

extended exposure to produced water. The CTA membrane exhibited no change in ATR-FTIR transmittance spectra (Fig. 9a), indicating exceptional robustness and resilience to chemical change of the polymeric active layer after exposure to produced water. The zeta potential of CTA changed slightly from pH 4 to pH 8 (Fig. 9b), suggesting a possible change to the membrane's electrokinetic properties; however, this slight change is likely due to the small concentration of negatively charged organic compounds irreversibly sorbed to the membrane surface. This phenomena was investigated by Childress et al. [29], who demonstrated the effect of organic compounds and divalent–organic compound complexations on membrane zeta potential.

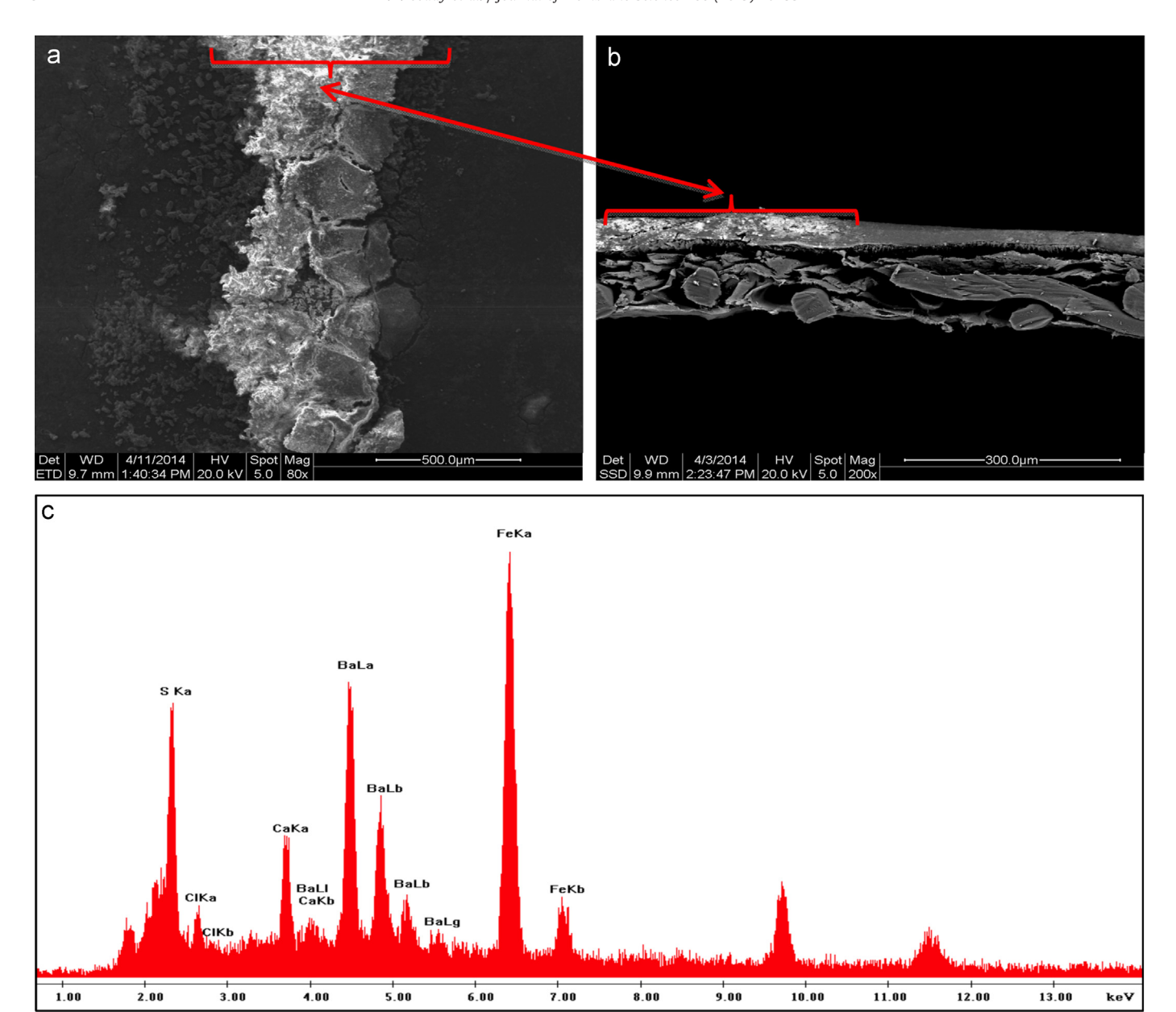


Fig. 8. ESEM micrograph of the TFC2 membrane (a) active layer and (b) cross section after fouling with produced water and subsequent chemical cleaning with EDTA. Irreversible organic fouling and inorganic scaling were observed on the membrane active layer, where the feed spacer contacts the membrane surface. (c) EDS spectrum of the fouling region on the membrane active layer indicates major ions present in the scaling layer.

Contrary to CTA, the TFC2 membrane exhibited substantial shifts in ATR-FTIR transmittance spectra (Fig. 9b). This indicates that the TFC2 polymer chemistry might be susceptible to chemical interaction with contaminants in the produced water. These findings might be supported by the significant decrease in zeta potential measurements of TFC2 after the majority of the fouling layer was chemically removed from the active layer. The zeta potential of the chemically cleaned TFC2 membrane was approximately 50 mV more negative than virgin samples (Fig. 9d) and even 25 mV more negative than the fouled membrane (\sim –30 mV at pH 7 (data not shown)). Furthermore, the zeta potential of the chemically cleaned TFC2 membrane closely resembled the ionization curve of an amphoteric surface from pH 3 to pH 10 (Fig. 9d). It is unlikely that such changes are induced by the chemical cleaning process due to similar changes in membrane physiochemical properties, regardless of chemical employed during membrane cleaning.

4. Conclusions

Results from the current study suggest that during treatment of produced water with no pretreatment: (1) FO membrane fouling is dominated by initial water flux and permeation drag in the short term; (2) physiochemical surface properties might play a more important role during membrane cleaning, especially under optimized conditions (e.g., suitable chemical cleaner versus osmotic backwashing); (3) long-term membrane fouling is dominated by foulant–foulant interactions after the formation of a cake layer, regardless of membrane type; (4) long-term fouling might be mitigated with suitable chemical pretreatment with appropriately selected anti-scalants or anti-foulants; and (5) long-term FO system performance might be better controlled with optimized hydrodynamic conditions near the membrane surface (i.e., feed flow velocity, module design, and membrane packing) and not by membrane selection. This is especially important given the recent

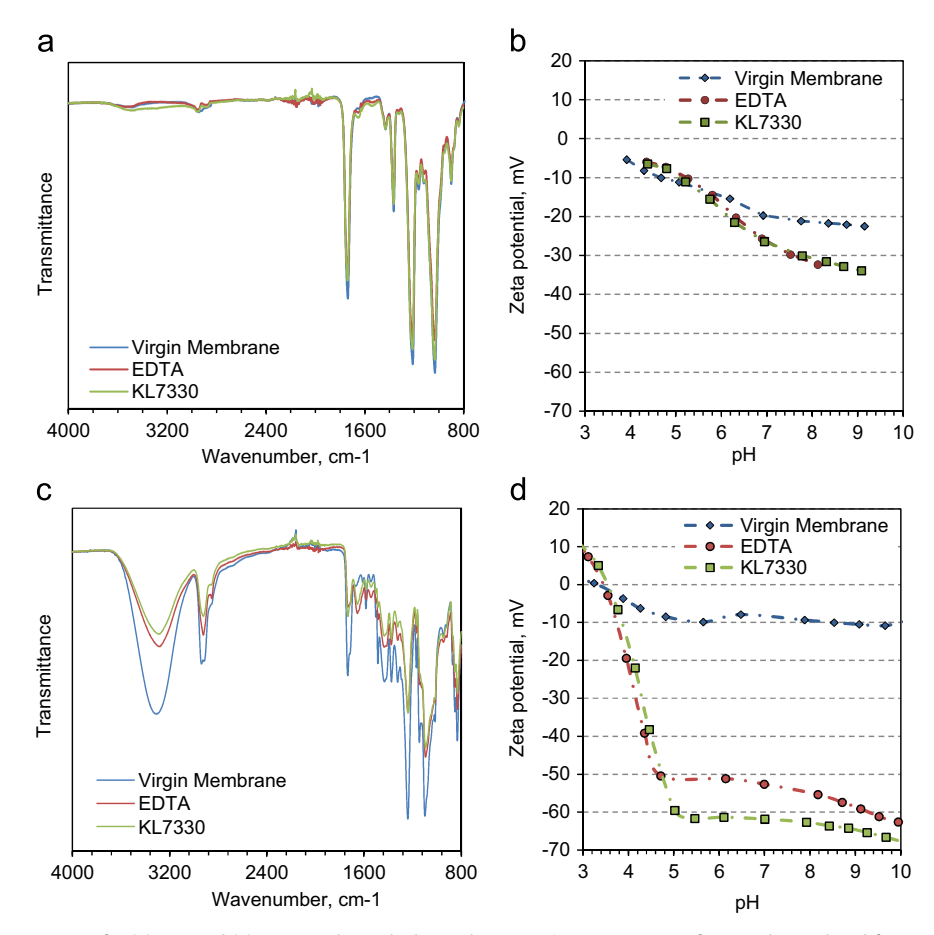


Fig. 9. ATR-FTIR transmittance spectra for (a) CTA and (c) TFC2. Each graph shows the transmittance spectrum for samples analyzed from a virgin membrane and fouled membranes chemically cleaned with EDTA and KL7330. Zeta potentials of virgin and chemically cleaned (b) CTA and (d) TFC2 membrane samples.

surge of interest in TFC membranes for treatment of complex feed streams with FO.

In general, the FO membranes demonstrated very high rejection of dissolved ions and organic compounds. While results from this study suggest that long-term rejection of feed stream contaminants might decline in the presence of a complex cake-layer at the membrane surface due to concentrative CP, the DS is of suitable quality for local reuse in subsequent hydraulic fracturing operations and for downstream desalination processes like RO. Further research and more well defined analytical techniques are needed to better understand, and accurately quantify the composition of dissolved organic compounds and nitrogen containing species that do permeate through the FO membranes into the DS. This is especially true given the complex nature and high TDS of most O&G production wastewaters, in addition to the highly concentrated DS streams that must be employed. Furthermore, accurate contaminant quantification is also of the utmost importance in cases where downstream desalination process might be employed and contaminants could become concentrated in the closed loop DS stream over time.

The chemical cleaning efficiency of EDTA was the highest throughout the study and was likely due to its high pH when mixed in solution and its chelating properties. Interestingly, the chemical cleaning efficiency of the TFC2 membrane remained consistent throughout the study and did not decline compared to CTA membrane. It is likely that the very smooth surface of TFC2 enabled higher chemical cleaning efficiency of the membrane, raising important questions regarding the potential economic tradeoffs between operating FO systems with lower flux CTA

membranes (resulting in lower fouling propensity) or with higher flux (and thus higher fouling rate) TFC membranes with potentially equal or superior cleaning properties to CTA. This is despite the fact that the contribution of the physiochemical surface properties of each membrane to its fouling propensity (compared to permeation drag) remains unclear given the complex nature of the feed stream.

Acknowledgments

Support of this investigation was provided by US Department of Energy/RPSEA project 10122-39. The authors would like to thank Hydration Technology Innovations for providing membranes for the study. Special thanks to Dr. Jonathan Brant, Satish Muthu, and Luke Ruff (University of Wyoming) for their technical advice and assistance with AFM measurements. The authors would also like to thank Estefani Bustos for her assistance with laboratory analyses and sample preparation. The CSM Undergraduate Research Fellowship Program is acknowledged for their financial support of Nohemi Almaraz during this investigation.

Appendix A. Supplementary material

Supplementary data associated with this article can be found in the online version at doi:10.1016/j.memsci.2015.03.059.

References

- K.B. Gregory, R.D. Vidic, D.A. Dzombak, Water management challenges associated with the production of shale gas by hydraulic fracturing, Elements 7.3 (2011) 181–186.
- [2] B.D. Coday, P. Xu, E.G. Beaudry, J. Herron, K. Lampi, N.T. Hancock, T.Y. Cath, The sweet spot of forward osmosis: treatment of produced water, drilling wastewater, and other complex and difficult liquid streams, Desalination 333 (2014) 23–35.
- [3] E. Barbot, N.S. Vidic, K.B. Gregory, R.D. Vidic, Spatial and temporal correlation of water quality parameters of produced waters from devonian-age shale following hydraulic fracturing, Environ. Sci. Technol. 47 (2013) 2562–2569.
- [4] M.E. Blauch, R.R. Myers, T. Moore, B.A. Lipinski, N.A. Houston, Marcellus shale post-frac flowback waters – where is all the salt coming from and what are the implications?, SPE Eastern Regional Meeting, Charleston, WV, 2009.
- [5] L.O. Haluszczak, A.W. Rose, L.R. Kump, Geochemical evaluation of flowback brine from Marcellus gas wells in Pennsylvania, USA, Appl. Geochem. 28 (2013) 55–61
- [6] B.D. Lutz, A.N. Lewis, M.W. Doyle, Generation, transport, and disposal of wastewater associated with Marcellus Shale gas development, Water Resourc. Res. 49 (2013) 647–656.
- [7] J.-P. Nicot, B.R. Scanlon, R.C. Reedy, R.A. Costley, Source and fate of hydraulic fracturing water in the Barnett shale: a historical perspective, Environ. Sci. Technol. 48 (2014) 2464–2471.
- [8] A. Vengosh, R.B. Jackson, N. Warner, T.H. Darrah, A. Kondash, A critical review of the risks to water resources from unconventional shale gas development and hydraulic fracturing in the United States, Environ. Sci. Technol. 48 (2014) 8334–8348.
- [9] M.S. Mauter, V.R. Palmer, Expert elicitation of trends in Marcellus oil and gas wastewater management, J. Environ. Eng. 140 (2014).
- [10] M.E. Blauch, Developing effective and environmentally suitable fracturing fluids using hydraulic fracturing flowback waters, in: SPE Unconventional Gas Conference, Pittsburgh, PA, 2010.
- [11] S. Rassenfoss, From flowback to fracturing: water recycling grows in the Marcellus Shale, J. Pet. Technol. 63 (2011) 48–51.
- [12] M. Zoback, S. Kitasei, B. Copithorne, Addressing the Environmental Risks From Shale Gas Development, Worldwatch Institute, Washington, D.C, 2010.
- [13] S. Kakadjian, J. Thompson, R. Torres, S. Trabelsi, F. Zamora, Y.A. Hamlat, Stable fracturing fluids from produced water, in: SPE Kuwait Oil and Gas Show and Conference, Mishref, Kuwait, 2013.
- [14] S. Ashkan Haghshenas, H.A. Nasr-El-Din, Effect of dissolved solids on reuse of produced water and proppant handling in hydraulic fracturing jobs in tight sand gas reservoirs, in: SPE Hydraulic Fracturing Technology Conference, The Woodlands, TX, 2014.
- [15] A. Haghshenas, H.A. Nasr-El-Din, Effect of dissolved solids on reuse of produced water at high temperature in hydraulic fracturing jobs, J. Nat. Gas Sci. Eng. 21 (2014) 316–325.
- [16] R. LeBas, P. Lord, D. Luna, T. Shahan, Development and use of high-TDS recycled produced water for crosslinked-gel-based hydraulic fracturing, in: SPE Hydraulic Fracturing Technology Conference, The Woodlands, TX, 2013.
- [17] T.Y. Cath, A.E. Childress, M. Elimelech, Forward osmosis: principles, applications, and recent developments, J. Membr. Sci. 281 (2006) 70–87.
- [18] D.L. Shaffer, L.H. Arias Chavez, M. Ben-Sasson, S. Romero-Vargas Castrillón, N.Y. Yip, M. Elimelech, Desalination and reuse of high-salinity shale gas produced water: drivers, technologies, and future directions, Environ. Sci. Technol. 47 (2013) 9569–9583.
- [19] T. Yun, J.-W. Koo, J. Sohn, S. Lee, Pressure assisted forward osmosis for shale gas wastewater treatment, Desalin. Water Treat. 54 (2014) 1–9.
- [20] R.L. McGinnis, N.T. Hancock, M.S. Nowosielski-Slepowron, G.D. McGurgan, Pilot demonstration of the NH₃/CO₂ forward osmosis desalination process on high salinity brines, Desalination 312 (2013) 67–74.
- [21] X.-M. Li, B. Zhao, Z. Wang, M. Xie, J. Song, L. Nghiem, T. He, C. Yang, C. Li, G. Chen, Water reclamation from shale gas drilling flow-back fluid using a novel forward osmosis-vacuum membrane distillation hybrid system, Water Sci. Technol. 69 (2014) 1036–1044.
- [22] N.R. Hutchings, E.W. Appleton, R.A. McGinnis, Making high quality frac water out of oilfield waste, in: SPE Annual Technical Conference and Exhibition, Florence, Italy, 2010.
- [23] K.L. Hickenbottom, N.T. Hancock, N.R. Hutchings, E.W. Appleton, E.G. Beaudry, P. Xu, T.Y. Cath, Forward osmosis treatment of drilling mud and fracturing wastewater from oil and gas operations, Desalination 312 (2013) 60–66.
- [24] B.D. Coday, B.G. Yaffe, P. Xu, T.Y. Cath, Rejection of trace organic compounds by forward osmosis membranes: a literature review, Environ. Sci. Technol. 48 (2014) 3612–3624.
- [25] T.-S. Chung, S. Zhang, K.Y. Wang, J. Su, M.M. Ling, Forward osmosis processes: yesterday, today and tomorrow, Desalination 287 (2012) 78–81.
- [26] K. Lutchmiah, A.R.D. Verliefde, K. Roest, L.C. Rietveld, E.R. Cornelissen, Forward osmosis for application in wastewater treatment: a review, Water Res. 58 (2014) 179–197.
- [27] B.D. Coday, D.M. Heil, P. Xu, T.Y. Cath, Effects of transmembrane hydraulic pressure on performance of forward osmosis membranes, Environ. Sci. Technol. 47 (2013) 2386–2393.
- [28] A. Tiraferri, N.Y. Yip, A.P. Straub, S. Romero-Vargas Castrillon, M. Elimelech, A method for the simultaneous determination of transport and structural

- parameters of forward osmosis membranes, J. Membr. Sci. 444 (2013) 523–538.
- [29] A.E. Childress, M. Elimelech, Effect of solution chemistry on the surface charge of polymeric reverse osmosis and nanofiltration membranes, J. Membr. Sci. 119 (1996) 253–268.
- [30] M. Elimelech, W.H. Chen, J.J. Waypa, Measuring the zeta (electrokinetic) potential of reverse osmosis membranes by a streaming potential analyzer, Desalination 95 (1994) 269–286.
- [31] J.A. Brant, A.E. Childress, Assessing short-range membrane-colloid interactions using surface energetics, J. Membr. Sci. 203 (2002) 257–273.
- [32] G. Hurwitz, G.R. Guillen, E. Hoek, Probing polyamide membrane surface charge, zeta potential, wettability, and hydrophilicity with contact angle measurements, J. Membr. Sci. 349 (2010) 349–357.
- [33] L. Gourley, M. Britten, S. Gauthier, Y. Pouliot, Characterization of adsorptive fouling on ultrafiltration membranes by peptides mixtures using contact angle measurements, J. Membr. Sci. 97 (1994) 283–289.
- [34] C. Bouchard, J. Jolicoeur, P. Kouadio, M. Britten, Study of humic acid adsorption on nanofiltration membranes by contact angle measurements, Can. J. Chem. Eng. 75 (1997) 339–345.
- [35] C. Van Oss, Acid-base interfacial interactions in aqueous media, Colloids Surf. A: Physicochem. Eng. Asp. 78 (1993) 1–49.
- [36] C.J. van Oss, Development and applications of the interfacial tension between water and organic or biological surfaces, Colloids Surf. B: Biointerfaces 54 (2007) 2–9.
- [37] N. Avraham, C. Dosoretz, R. Semiat, Osmotic backwash process in RO membranes, Desalination 199 (2006) 387–389.
- [38] K. Spiegler, J. Macleish, Molecular (osmotic and electro-osmotic) backwash of cellulose acetate hyperfiltration membranes, J. Membr. Sci. 8 (1981) 173–192.
- [39] M. Park, J.H. Kim, Numerical analysis of spacer impacts on forward osmosis membrane process using concentration polarization index, J. Membr. Sci. 427 (2013) 10–20.
- [40] J. Ren, J.R. McCutcheon, A new commercial thin film composite membrane for forward osmosis, Desalination 343 (2014) 187–193.
- [41] N. El Shaari, M. Kedzierski, T. Gorham, Quantifying guar polymer recovery post hydraulic fracturing to determine the degree of fracture cleanup: a field study of the point of rocks formation california, in: SPE Western Regional Meeting, Irvine, CA, 2005.
- [42] R. Barati, J.T. Liang, A review of fracturing fluid systems used for hydraulic fracturing of oil and gas wells, J. Appl. Polym. Sci. 131 (2014).
- [43] S. Hong, M. Elimelech, Chemical and physical aspects of natural organic matter (NOM) fouling of nanofiltration membranes, J. Membr. Sci. 132 (1997) 159–181.
- [44] C.Y. Tang, Q. She, W.C. Lay, R. Wang, A.G. Fane, Coupled effects of internal concentration polarization and fouling on flux behavior of forward osmosis membranes during humic acid filtration, J. Membr. Sci. 354 (2010) 123–133.
- [45] Q. Li, Z. Xu, I. Pinnau, Fouling of reverse osmosis membranes by biopolymers in wastewater secondary effluent: role of membrane surface properties and initial permeate flux, J. Membr. Sci. 290 (2007) 173–181.
- [46] B. Mi, M. Elimelech, Chemical and physical aspects of organic fouling of forward osmosis membranes, J. Membr. Sci. 320 (2008) 292–302.
- [47] V. Parida, H.Y. Ng, Forward osmosis organic fouling: effects of organic loading, calcium and membrane orientation, Desalination 312 (2013) 88–98.
- [48] Y. Gu, Y.-N. Wang, J. Wei, C.Y. Tang, Organic fouling of thin-film composite polyamide and cellulose triacetate forward osmosis membranes by oppositely charged macromolecules, Water Res. 47 (2013) 1867–1874.
- [49] A. Tiraferri, Y. Kang, E.P. Giannelis, M. Elimelech, Superhydrophilic thin-film composite forward osmosis membranes for organic fouling control: fouling behavior and antifouling mechanisms, Environ. Sci. Technol. 46 (2012) 11135–11144.
- [50] J. Mansouri, S. Harrisson, V. Chen, Strategies for controlling biofouling in membrane filtration systems: challenges and opportunities, J. Mater. Chem. 20 (2010) 4567–4586.
- [51] E.M. Vrijenhoek, S. Hong, M. Elimelech, Influence of membrane surface properties on initial rate of colloidal fouling of reverse osmosis and nanofiltration membranes, J. Membr. Sci. 188 (2001) 115–128.
- [52] M.M. Motsa, B.B. Mamba, A. D'Haese, E. Hoek, A.R. Verliefde, Organic fouling in forward osmosis membranes: The role of feed solution chemistry and membrane structural properties, J. Membr. Sci. 460 (2014) 99–109.
- [53] B.D. Coday, T. Luxbacher, A.E. Childress, N. Almaraz, P. Xu, T.Y. Cath, Indirect determination of zeta potential at high ionic strength: Specific application to semipermeable polymeric membranes. I. Membr. Sci. 478 (2015) 58–64.
- [54] J.R. McCutcheon, M. Elimelech, Influence of concentrative and dilutive internal concentration polarization on flux behavior in forward osmosis, J. Membr. Sci. 284 (2006) 237–247.
- [55] E.M. Hoek, S. Bhattacharjee, M. Elimelech, Effect of membrane surface roughness on colloid-membrane DLVO interactions, Langmuir 19 (2003) 4836–4847.
- [56] B. Mi, M. Elimelech, Organic fouling of forward osmosis membranes: fouling reversibility and cleaning without chemical reagents, J. Membr. Sci. 348 (2010) 337–345
- [57] E.M. Hoek, M. Elimelech, Cake-enhanced concentration polarization: a new fouling mechanism for salt-rejecting membranes, Environ. Sci. Technol. 37 (2003) 5581–5588.
- [58] R.W. Holloway, A.S. Wait, A.F. da Silva, J. Herron, M.D. Schutter, K. Lampi, T.Y. Cath, Long-term pilot scale investigation of novel hybrid ultrafiltrationosmotic membrane bioreactors, Desalination 363 (2015) 64–74.

- [59] N.T. Hancock, T.Y. Cath, Solute coupled diffusion in osmotically driven membrane processes, Environ. Sci. Technol. 43 (2009) 6769–6775.
- [60] N. Ferretto, M. Tedetti, C. Guigue, S. Mounier, R. Redon, M. Goutx, Identification and quantification of known polycyclic aromatic hydrocarbons and pesticides in complex mixtures using fluorescence excitation-emission matrices and parallel factor analysis, Chemosphere 107 (2014) 344–353.
- [61] N.T. Hancock, P. Xu, M.J. Roby, J.D. Gomez, T.Y. Cath, Towards direct potable reuse with forward osmosis: technical assessment of long-term process performance at the pilot scale, J. Membr. Sci. 445 (2013) 34–46.
- [62] K.G. Dahm, C.M. Van Straaten, J. Munakata-Marr Jr, E. Drewes, Identifying well contamination through the use of 3-D fluorescence spectroscopy to classify coalbed methane produced water, Environ. Sci. Technol. 47 (2012) 649–656.
- [63] C.A. Stedmon, S. Markager, R. Bro, Tracing dissolved organic matter in aquatic environments using a new approach to fluorescence spectroscopy, Mar. Chem. 82 (2003) 239–254.
- [64] P.G. Coble, Characterization of marine and terrestrial DOM in seawater using excitation-emission matrix spectroscopy, Mar. Chem. 51 (1996) 325–346.